Using Self-Assembly To Control the Structure of DNA Monolayers on Gold: A Neutron Reflectivity Study

Rastislav Levicky,[†,‡] Tonya M. Herne,[†] Michael J. Tarlov,*[,†] and Sushil K. Satija[§]

Contribution from the Chemical Science & Technology Laboratory and NIST Center for Neutron Research, National Institute of Standards and Technology, Gaithersburg, Maryland 20899

Received June 1, 1998

Abstract: Neutron reflectivity was used to determine the concentration profiles of oligomeric DNA monolayers on gold in high salt concentrations (1 M NaCl). These monolayers are of interest as models for DNA probe systems used in diagnostic devices. To facilitate its attachment, the DNA was functionalized at the 5′ end with a thiol group connected to the oligonucleotide by a hexamethylene linker. Concentration profiles determined from neutron reflectivity indicate that adsorbed layers of single-stranded DNA (HS-ssDNA) on bare gold are compact, suggesting the presence of multiple contacts between each DNA strand and the surface. After treatment with mercaptohexanol, a short alkanethiol with a terminal hydroxy group, the DNA "stands up" and extends farther into the solvent phase. These changes are consistent with the DNA remaining attached through its thiol end group while contacts between DNA backbones and the surface are prevented by the formation of a mercaptohexanol monolayer. The end-tethered HS-ssDNA layer readily hybridized to its complementary sequence, resulting in DNA helices with a preferred orientation toward the substrate normal.

Introduction

The interaction between DNA-functionalized surfaces and free oligonucleotides in solution is important in detection and diagnostic processes. For instance, high-performance, array-based genetic diagnostics rely on the binding of analyte nucleic acids by surface-tethered DNA strands.[1] Such devices show tremendous promise for medical, pharmaceutical, forensic, and other applications. DNA-functionalized surfaces have also been employed for chiral and other high-affinity separations involving small molecules and proteins.[2] When attached to colloidal particles, DNA has been used as an organizational template for the rational assembly of larger structures.[3] A common concern in these and related applications is the conformation of the DNA on the surface. For example, the DNA must remain capable of unhindered, specific interaction with oligonucleotides in solution.

Previous work on characterizing the conformation of surface-bound oligonucleotides has included the application of hydroxyl radical footprinting,[4] direct nonradiative energy transfer,[5] and two-color surface-plasmon resonance.[6] These techniques provided important insights into the structure of surface-bound DNA. For instance, adsorbed DNA extended farther into the solvent phase when the adsorbing surface was electrostatically repulsive[4] or when high DNA surface densities were employed.[4,5] Nevertheless, questions about the distribution of DNA segments in the vicinity of the surface and how it may be controlled remain virtually unexplored.

In an earlier article,[7] we reported the preparation of mixed monolayers of 6-mercapto-1-hexanol (MCH) and oligomeric single-stranded DNA (ssDNA) on gold surfaces. Although MCH effectively displaced adsorbed ssDNA from the gold surface, functionalization of the ssDNA with a thiol end group caused a significant DNA fraction to remain bound. These observations suggested that the HS-ssDNA was primarily tethered through the thiol end groups and that MCH blocked nonspecific contacts between DNA backbones and the surface (Figure 1). Such conformations of the HS-ssDNA, in which only one end of the DNA strands is bound to the substrate, were anticipated to be most favorable for the subsequent binding of analyte single-stranded oligonucleotides. Indeed, radiolabeling measurements demonstrated that the mixed HS-ssDNA/MCH monolayers exhibited nearly 100% binding efficiencies toward analyte oligonucleotides carrying the complementary base sequence.[7]

In this article, we extend the earlier study to report the in situ visualization of the conformational changes of surface-tethered, oligomeric HS-ssDNA arising from the MCH treatment and from hybridization. The DNA concentration profiles in the

* To whom correspondence should be addressed. NIST Bldg. 221/A303, Gaithersburg, MD 20899. Phone: (301) 975-2058. Fax: (301) 869-5924. E-mail: michael.tarlov@nist.gov.

† Chemical Science & Technology Laboratory.

‡ Present address: Department of Chemical Engineering & Applied Chemistry, Columbia University, New York, NY 10027.

§ NIST Center for Neutron Research.

(1) (a) Fodor S. P. A. *Science* **1997**, *277*, 393−395. (b) Chee, M.; Yang, R.; Hubbell, E.; Berno, A.; Huang, X. C.; Stern, D.; Winkler, J.; Lockhart, D. J.; Morris, M. S.; Fodor, S. P. A. *Science* **1996**, *274*, 610−614. (c) Mirzabekov, A. D. *Trends Biotechnol*. **1994**, *12*, 27−32. (d) Dubiley, S.; Kirillov, E.; Lysov, Y.; Mirzabekov, A. *Nucleic Acids Res.* **1997**, *25*, 2259−2265. (e) Southern, E. M.; Case-Green, S. C.; Elder, J. K.; Johnson, M.; Mir, K. U.; Wang, L.; Williams, J. C. *Nucleic Acids Res.* **1994**, *22*, 1368−1373. (f) Maskos, U.; Southern, E. M. *Nucleic Acids Res.* **1992**, *20*, 1675−1684.

(2) (a) Tuerk, C.; Gold, L. *Science* **1990**, *249*, 505−510. (b) Gold, L.; Polisky, B.; Uhlenbeck, O.; Yarus, M. *Annu. Rev. Biochem.* **1995**, *64*, 763−797.

(3) (a) Elghanian, R.; Storhoff, J. J.; Mucic, R. C.; Letsinger, R. L.; Mirkin, C. A. *Science* **1997**, *277*, 1078−1081. (b) Alivisatos, A. P.; Johnsson, K. P.; Peng, X.; Wilson, T. E.; Loweth, C. J.; Bruchez, M. P., Jr.; Schultz, P. G. *Nature* **1996**, *382*, 609−611.

(4) Walker, H. W.; Grant, S. B. *Langmuir* **1995**, *11*, 3772−3777.

(5) Charreyre, M.-T.; Tcherkasskaya, O.; Winnik, M. A.; Hiver, A.; Delair, T.; Cros, P.; Pichot, C.; Mandrand, B. *Langmuir* **1997**, *13*, 3103−3110.

(6) Peterlinz, K. A.; Georgiadis, R. M.; Herne, T. M.; Tarlov, M. J. *J. Am. Chem. Soc.* **1997**, *119*, 3401−3402.

(7) Herne, T. M.; Tarlov, M. J. *J. Am. Chem. Soc.* **1997**, *119*, 8916−8920.

S0002-7863(98)01897-6
Published on Web 09/09/1998

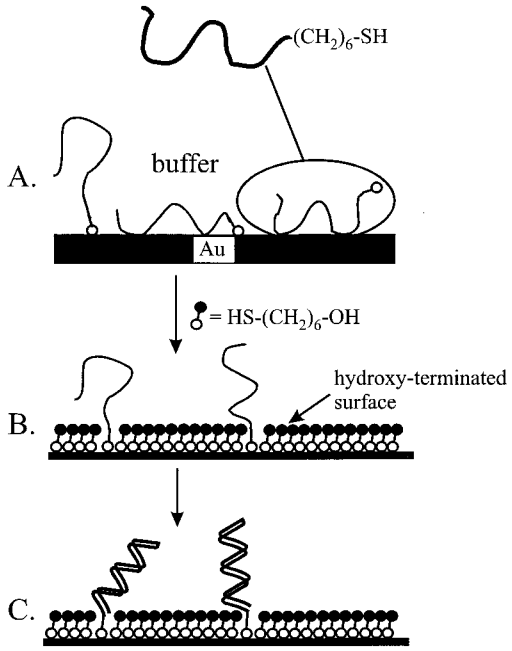

Figure 1. (A) Single-stranded DNA (HS-ssDNA) which adsorbs to the gold substrate through the thiol end group as well as through backbone/substrate contacts. A multitude of adsorption states exists. (B) After the formation of a mercaptohexanol (MCH) monolayer that prevents contacts between the DNA backbone and the substrate, the HS-ssDNA is left attached by the thiol end. (C) The end-tethered HS-ssDNA after hybridization to complementary oligonucleotides.

vicinity of the substrate were determined from neutron reflectivity measurements. Neutron reflectivity enables depth-profiling of planar-stratified structures with Angstrom-level resolution.[8] For instance, HS-ssDNA is observed to pass from a compact to an extended configuration following the MCH treatment. From the concentration profiles, the location and stratification of the DNA and MCH within the monolayer can be determined. In addition, information about interactions that influence the DNA layer structure can be deduced.

Experimental Section

Substrate Preparation. One-side polished, ⟨111⟩ cut silicon wafers 13-mm thick and 100 mm in diameter were used as substrates. Immediately prior to deposition of metal overlayers, the wafers were cleaned under a 80 °C "piranha" solution consisting of 70% concentrated sulfuric acid and 30% hydrogen peroxide (30% H_2O_2 in H_2O) for 15 min, thoroughly rinsed with 18 MΩ cm water, and dried under a nitrogen stream. *WARNING! Piranha solution is extremely oxidizing, reacts violently with organics, and should only be stored in loosely tightened containers to avoid buildup of pressure.* A 1-nm-thick adhesion layer of chromium was deposited at a rate of 0.1 nm/s, followed by a 4.5 nm layer of gold at 0.15 nm/s. The resultant gold films were sufficiently smooth for neutron reflectivity measurements (larger film thickness results in increased surface roughness).[9] All substrates were used within 10 h. Immediately prior to DNA adsorption, the substrates were placed for 12 min into a UV/ozone cleaner (Boekel 135500).[10] To minimize adventitious surface contamination, throughout the experiments the samples were kept under deionized water or a buffer solution and were not allowed to dry.

Adsorption of Thiol-Derivatized HS-ssDNA Oligonucleotides. Single-stranded, 25-base-long DNA oligonucleotides, designated HS-ssDNA, were adsorbed from 1 or 1.9 μM solutions in 1 M potassium phosphate buffer, pH 6.7, for 90 min. The oligonucleotide structure was 5′-HS-$(CH_2)_6$-CAC GAC GTT GTA AAA CGA CGG CCA G-3′ (C = cytosine, G = guanine, A = adenine, T = thymine). The thiol end group is at the 5′ end. All oligonucleotides used in this study were purchased from Research Genetics.[10] After adsorption and rinsing with 18 MΩ cm water, the samples were characterized in situ by neutron reflectivity (see below).

Formation of Mixed HS-ssDNA/Mercaptohexanol Monolayers. MCH was purified by flash chromatography. Substrates bearing preadsorbed HS-ssDNA were immersed under a 1 mM aqueous solution of MCH for 5 min and thoroughly rinsed. The thiol group on the MCH chemically adsorbs to the gold surface, creating a mixed monolayer of HS-ssDNA and MCH.[6,7]

Hybridization of Surface-Tethered HS-ssDNA Oligonucleotides to ssDNA-C. The hybridization of surface-bound HS-ssDNA to complementary oligonucleotides (ssDNA-C: 5′-CTG GCC GTC GTT TTA CAA CGT CGT G-3′) was performed in 1.4 μM ssDNA-C solutions in TE−1 M NaCl buffer at 37 °C for 90 min (TE buffer: 10 mM tris-HCl, 1 mM EDTA, 1 M NaCl, pH 7.0). Following hybridization, the samples were rinsed with TE−1 M NaCl buffer and cooled to 22 °C, and the reflectivity data were collected in situ under the buffer solution.

Neutron Reflectivity Measurements. Neutron reflectivity experiments were performed on the NG7 reflectometer at the National Institute of Standards and Technology in Gaithersburg, MD. The experiments employed 0.477-nm-wavelength neutrons. Data were collected up to a momentum transfer of $q_z = 1.5$ nm^{-1} ($q_z = 4\pi \sin(\theta/\lambda)$, where θ is the grazing angle of incidence and λ is the neutron wavelength). A temperature-controlled solvent cell held the samples during the measurements. Parts contacting the sample surface or the buffer solution were constructed of poly(tetrafluoroethylene) or fused silica and were cleaned overnight in chromic acid. All measurements were performed under TE−1 M NaCl buffer, pH 7.0, at 22 ± 0.1 °C. For one set of experiments, the TE−1 M NaCl buffer was prepared using glass-distilled D_2O (Cambridge Isotope Laboratories)[10] to enhance neutron contrast at the buffer/MCH monolayer interface. All scans were checked for reproducibility by repeating the first half of the scan 2 h later. The two data sets were always superimposed. Off-specular measurements, obtained by tilting the sample about the specular position, showed that in aqueous H_2O buffer the specular signal beyond $q_z = 1.2$ nm^{-1} became difficult to distinguish from background scattering. Under D_2O, the incoherent background from the buffer was weaker, and the specular signal could be resolved at least to $q_z = 1.5$ nm^{-1}. Accordingly, data were analyzed up to these maximal q_z values.

Neutron Reflectivity Analyses. Experimental reflectivities were corrected for background and normalized to the incident beam intensity prior to analysis. The sample structure was determined by fitting calculated reflectivities from trial structural models to the experimental data.[8] The sample structures were expressed in terms of their scattering length density (SLD) profiles as a function of the distance z from the substrate. The SLD profile is related to the refractive index profile $n(z)$

$$n(z) = 1 - (\lambda^2/2\pi)\mathrm{SLD}(z)$$

Trial SLD profiles are generated by piecewise, end-to-end splicing of simple functions.[11] Each layer of the sample (i.e., gold film, DNA monolayer, or substrate oxide) is represented by a function, and the function is defined by variables such as its z-extent (width) and the value and variation in SLD across the region it represents. The interfaces in the film are located at the nodes at which two functions (layers) meet, and the interfacial width is adjusted to the desired value by convoluting the SLD profile with a Gaussian smearing function at the location of the interface. Once a trial refractive index profile has been constructed, the reflectivity is calculated over the q_z range of interest using standard procedures from optics. These procedures

(8) (a) Russell, T. P. *Mater. Sci. Rep.* **1990**, *5*, 171−271. (b) Penfold, J.; Thomas, R. K. *J. Phys.: Condens. Matter C* **1990**, *2*, 1369−1412.

(9) Vázquez, L.; Salvarezza, R. C.; Herrasti, P.; Ocón, P.; Vara, J. M.; Arvia, A. J. *Surf. Sci.* **1996**, *345*, 17−26.

(10) Certain commercial products and instruments are identified to adequately specify the experimental procedure. In no case does such identification imply endorsement by the National Institute of Standards and Technology.

(11) Levicky, R. Ph.D. Dissertation, University of Minnesota, 1996.

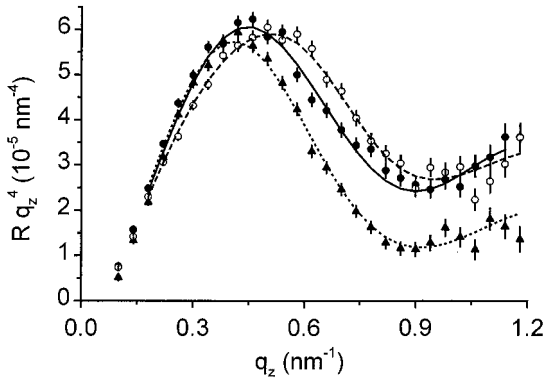

Figure 2. Experimental (points) and calculated (lines) reflectivities for a DNA monolayer on gold. The data were obtained under TE−1 M NaCl buffer prepared with H_2O. The calculated reflectivities correspond to the scattering length density (SLD) profiles shown in Figure 3. Above $q_z > 1$ nm^{-1} where the signal-to-noise worsens, some of the data exhibit artifacts arising from the background correction algorithm. Triangles and dotted line: Adsorbed HS-ssDNA monolayer (Figure 1A). Filled circles and solid line: Mixed HS-ssDNA/MCH monolayer (Figure 1B). Open circles and dashed line: Mixed HS-ssDNA/MCH monolayer after hybridization (Figure 1C).

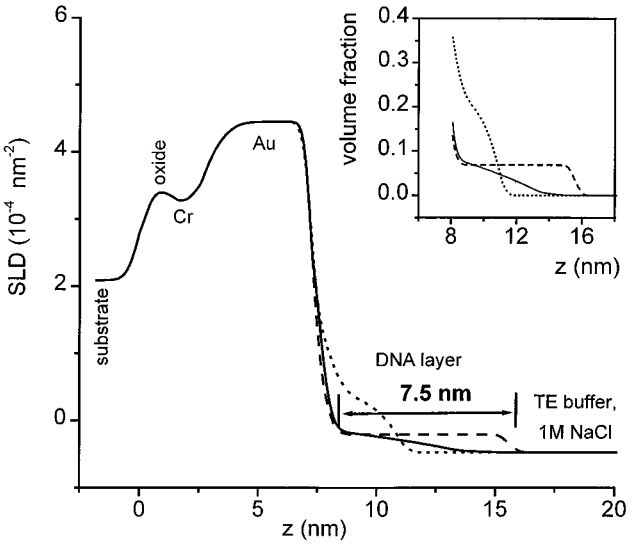

Figure 3. SLD profiles determined from the experimental reflectivities in Figure 2. Dotted line: Adsorbed HS-ssDNA monolayer (Figure 1A). Solid line: Mixed HS-ssDNA/MCH monolayer (Figure 1B). Dashed line: Mixed HS-ssDNA/MCH monolayer after hybridization (Figure 1C). Inset: Corresponding DNA volume fraction profiles.

involve discretizing the SLD into 0.1-nm-wide slivers and using a recursive algorithm[8,12] to calculate the reflectivity. The instrumental resolution, as defined by the beam monochromaticity and collimation, is included by convoluting the calculated reflectivity curve with a Gaussian smearing function. The goodness of fit between the experimental and calculated reflectivity curves is measured by a χ^2 statistic.[13] When the variables specifying the SLD profile are varied to improve the agreement between the calculated and experimental reflectivities, the χ^2 value is minimized to determine the best fit. Typical final values of χ^2 are ∼2.5. Surface coverages are determined by numerical integration of the appropriate portions of the SLD profile, which is directly related to the sample composition.[14]

Results and Discussion

One of the goals of the present work was to obtain an understanding of the in situ conformation of surface-bound HS-ssDNA on gold and to determine how it is influenced by co-assembly of MCH. To address these issues, two samples were characterized at each stage in Figure 1. The conclusions drawn from both samples were the same. One set of the reflectivity R vs q_z curves is displayed in Figure 2. The points are experimental data, the lines are calculated fits. When q_z^4R vs q_z is plotted, the underlying Fresnel dependence[8] $R \approx q_z^{-4}$ corresponding to reflection from an infinitely sharp interface between two semi-infinite media is removed and the trends arising from changes in the sample structure are more clearly visualized.

The SLD profiles corresponding to the calculated reflectivities are shown in Figure 3. The interface between the bulk silicon substrate and the native silicon oxide layer is located at $z = 0$ nm. As indicated in Figure 3, the leftmost layer represents the silicon substrate (SLD $= 2.09 \times 10^{-4}$ nm^{-2}), followed by about a 1.5-nm-thick native oxide layer, a 1.0-nm-wide chromium adhesion layer, a 4.5-nm-thick gold layer (SLD $= 4.5 \times 10^{-4}$ nm^{-2}), a region in which the DNA/MCH monolayer resides, and the bulk buffer solution (TE−1 M NaCl buffer, SLD $= -0.46 \times 10^{-4}$ nm^{-2}). The SLD of the gold layer coincides with the value for bulk gold,[15] and the root-mean-square (rms) roughness of the gold/buffer interface is 0.5 ± 0.1 nm. The region containing the DNA begins near $z = 8.0$ nm. In this region, the deviation of the SLD from the pure buffer value is proportional to the local DNA volume fraction.[14] The corresponding DNA volume fraction profiles are displayed in the inset.

During data analysis, the SLD values of the substrate and aqueous buffer were fixed at bulk values. The SLD and thickness of the three box functions representing the SiO_x, Cr, and Au layers and the widths of interfaces in the Si/SiO_x/Cr/Au region were varied subject to the constraint that the same values satisfy all three data sets in Figure 2. This self-consistency check is appropriate because changes in the DNA monolayer should not perturb the underlying substrate structure. Therefore, the shifts in the reflectivity curves in Figure 2 were accounted for by varying the SLD profile in the region of the DNA monolayer only. The SLD of the DNA layer was represented by SLD(z') $= C_1 + C_2[1 - (z'/H)^n]$, where C_1 is fixed at the buffer SLD value, z' is the distance from the gold layer surface, and H is the width of the layer. The form of this function is similar to those derived in theoretical studies on end-tethered polymer assemblies.[16] H, C_2, n, and the widths of the interfaces around the DNA layer were optimized for best fit to the reflectivity data. More complex models were also tested; for instance, the DNA layer was represented by two functions to impart greater flexibility to its SLD profile. However, these attempts did not reveal any new structural features and converged to profiles that were very similar to those obtained with the simpler, one-function construction.

The profile of the initially adsorbed HS-ssDNA monolayer is depicted by the dotted line in Figure 3. The volume fraction decreases from approximately 0.25 at $z = 9$ nm to 0 at $z = 12$

(12) Parratt, L. G. *Phys. Rev.* **1954**, *95*, 359.

(13) $\chi^2 = P^{-1}\sum_i(R_{ical} - R_{iexp})^2/\delta R_i^2$ where P is the number of data points, R_{ical} is the calculated reflectivity for data point i, and R_{iexp} is the experimentally measured reflectivity with a standard deviation δR_i.

(14) SLD $= \sum\Phi_i$ SLD$_i$, where Φ_i is the volume fraction of species i and SLD$_i$ is the value for the pure compound as calculated from tabulated elemental scattering lengths.

(15) The agreement with the value for bulk gold indicates that the gold film is continuous. However, we cannot rule out variations of a few percent (∼±3%) in the SLD of the gold layer.

(16) (a) Halperin, A.; Tirrell, M.; Lodge, T. P. *Adv. Polym. Sci.* **1992**, *100*, 31−71. (b) Milner, S. T. *Science* **1991**, *251*, 905−914. (c) Szleifer, I.; Carignano, M. A. In *Advances in Chemical Physics*; Prigogine, I., Rice, S. A., Eds.; John Wiley & Sons, Inc.: New York, 1996; pp 165−260.

nm.[17] The coverage of HS-ssDNA is determined by integrating the volume fraction profile and is found to be 0.8 mg/m^2 ($\sim 6 \times 10^{12}$ chains/cm^2).[18] The coverage can be compared to the value of 9×10^{12} chains/cm^2 determined previously for a similar sample using surface-plasmon resonance spectroscopy (SPR).[6] It is interesting to contrast the width of the volume fraction profile with the characteristic size of an isolated DNA strand in solution. For instance, such comparison can indicate whether the chains become "flattened" from their solvated state after adsorption. In solution, the characteristic size of an isolated polymer is given by the radius of gyration R_g,[19] which represents the rms distance of a backbone segment from the polymer's center of mass. Tinland et al.[20] measured single-stranded DNA hydrodynamic radii. In the high salt limit, R_g was estimated as $R_g = 0.38N^{1/2}$ nm, where N is the number of bases in the DNA chain. Because the segments of an isolated chain are isotropically distributed in space, the component of R_g along a unique coordinate direction (x, y, or z) is $R_g/3^{1/2}$. For an isolated 25-base-long ssDNA, we obtain $R_{gz} = 1.1 \pm 0.1$ nm. This would be the expected z-rms thickness[21] of the HS-ssDNA layer if the DNA strands did not deform upon adsorption. In contrast, the actual z-rms thickness of the adsorbed HS-ssDNA monolayer is 0.7 nm. The smaller thickness indicates that the adsorbed chains are flattened relative to the isolated solution state. We believe the flattened configurations indicate the presence of multiple adsorption contacts between a strand of HS-ssDNA and the gold.

After the adsorbed DNA monolayer was exposed to the MCH solution, the reflectivity curve shifted upward (Figure 2, circles) and the HS-ssDNA extended farther out into the buffer (Figure 3, solid line). The increase in the thickness of the HS-ssDNA profile indicates that the chains are lifted off the substrate. This process corresponds to going from model A to B in Figure 1, in which the formation of an MCH monolayer creates a hydroxy-terminated surface to which ssDNA does not strongly adsorb.[7] The z-rms width increased from 0.7 to 1.4 nm, exceeding the isolated chain R_{gz} (1.1 nm) by $\sim$25%. The DNA surface coverage is 0.4 mg/m^2 ($\sim 3 \times 10^{12}$ chains/cm^2), corresponding to $\sim$6-nm lateral interchain spacing. Only about 50% of the strands remained bound after the MCH treatment, an observation that is consistent with previous SPR measurements.[6]

An interesting issue to consider is the influence of interactions among neighboring ssDNA strands on the layer structure. In a buffer with this ionic strength, the Debye length is 3 Å, so the range of electrostatic forces is short compared to interchain spacing. Therefore, electrostatic interchain repulsions are expected to be weak. Interchain steric effects should become pronounced above the chain-overlap surface density $1/\pi R_g^2$ [16,22] or 0.09 chains/nm^2. The experimental surface density was 0.03 chains/nm^2; therefore, steric interchain repulsions should also be weak. Accordingly, at least under the high salt conditions of this study, the ssDNA strands should approximate surface-tethered coils with weak lateral interactions. We should point out that the greater z-rms thickness of the layer relative to the bulk solution R_{gz} does not imply that interstrand repulsions are causing the DNA chains to stretch. In fact, the modest increase largely can be attributed to confining effects caused by the impenetrable substrate.[22a,23] For instance, Monte Carlo simulations[23] of neutral (uncharged) isolated chains reported a $\sim$20% increase in the end-to-end dimension when the chains were tethered by one end to an impenetrable surface.

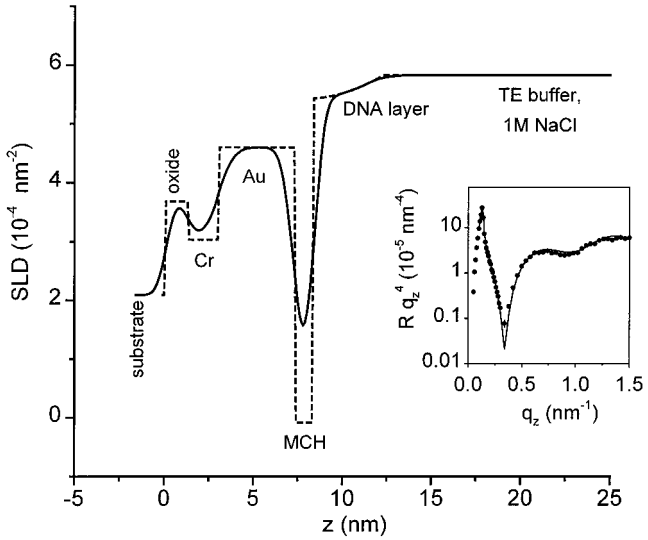

Figure 4. Solid line: SLD profile for a mixed HS-ssDNA/MCH monolayer (Figure 1B) immersed in a TE−1 M NaCl buffer prepared with D_2O. Dashed line: Same SLD profile but without interfacial smearing. A $\sim$1.0-nm-thick layer with an SLD corresponding to that of MCH is next to the gold film. Inset: Experimental (points) and calculated (line) reflectivities.

To further characterize the MCH monolayer, measurements were performed on a separate sample under a TE−1 M NaCl buffer prepared with D_2O. The contrast between MCH (MCH: SLD $= -0.17 \times 10^{-4}$ nm^{-2}) and the D_2O buffer (D_2O buffer: SLD $= 5.8 \times 10^{-4}$ nm^{-2})[24] is stronger than that between MCH and the H_2O buffer (H_2O buffer: SLD $= -0.46 \times 10^{-4}$ nm^{-2}). When the interface between the buffer and the MCH monolayer was made visible, the improved contrast enabled the width and location of the MCH monolayer to be resolved. Figure 4 plots the SLD profile for a mixed HS-ssDNA/MCH monolayer under a D_2O buffer (solid line). To clearly show the various layers present, the SLD profile is also plotted without interfacial smearing (dashed line). A 1.0-nm-wide layer with an SLD corresponding to that of MCH is located between the gold film and the DNA. This width should correspond to the alkane chain portion of the MCH monolayer, which is easy to distinguish because of its strong contrast. On the other hand, the outer MCH monolayer region in which the terminal hydroxy groups reside should be less distinguishable because exchange

(17) Previously, using two-color surface-plasmon resonance (SPR) measurements,[6] the thickness of a similar layer of adsorbed HS-ssDNA was reported to be $\sim$17 nm (corresponding to the unlikely situation of perpendicular, fully extended DNA chains at subsaturation coverage). The present experiments conclusively rule out such a large thickness. The SPR calculation involved assumptions as to the optical properties of the adsorbed layer, which may have led to the overestimation of the layer thickness.

(18) The calculation of the coverages accounted for the presence of one Na^+ counterion per DNA phosphate group. From the sensitivity of the calculated fits, we estimate an uncertainty in coverages of $\pm$10%.

(19) Fujita, H. *Polymer Solutions*; Elsevier: New York, 1990.

(20) Tinland, B.; Pluen, A.; Sturm, J.; Weill, G. *Macromolecules* **1997**, *30*, 5763−5765. The ssDNA persistence length was taken to be 1.0 nm. Tinland et al. estimated the persistence length to lie between 0.8 and 1.3 nm, which corresponds to less than $\pm$15% uncertainty in R_g.

(21) The z-rms thickness of the DNA layer is $[\langle z^2\rangle - \langle z\rangle^2]^{1/2}$, where $\langle\ \rangle$ denotes an average with respect to the DNA volume fraction profile $\Phi(z)$ [e.g., $\langle z^2\rangle = \int z'^2\Phi(z')\,dz/\int\Phi(z')\,dz$]. The definition of the z-rms thickness is consistent with that of R_g for a macromolecule in solution, see ref 19.

(22) (a) Kent, M. S.; Lee, L. T.; Factor, B. J.; Rondelez, F.; Smith, G. S. *J. Chem. Phys.* **1995**, *103*, 2320−2342. (b) Auroy, P.; Auvray, L.; Léger, L. *Phys. Rev. Lett.* **1991**, *66*, 719−721. (c) Karim, A.; Satija, S. K.; Douglas, J. F.; Ankner, J. F.; Fetters, L. J. *Phys. Rev. Lett.* **1994**, *73*, 3407−3410.

(23) Hahn, T. D.; Kovac, J. *Macromolecules* **1990**, *23*, 5153−5154.

(24) If absolutely no H_2O were present in the buffer, the SLD of the D_2O−1 M NaCl buffer should be 6.35×10^{-4} nm^{-2}. The lower value in the experiments (5.8×10^{-4} nm^{-2}) is due to H_2O remnants from rinsing steps which used 18 MΩ cm H_2O.

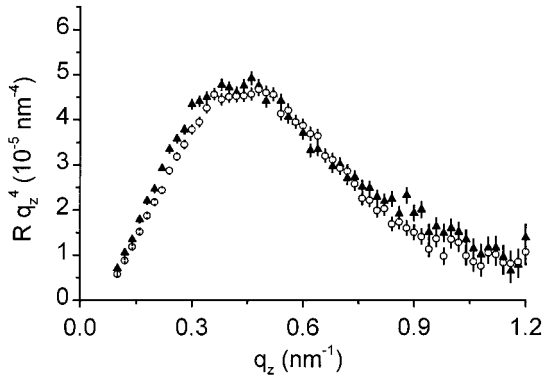

Figure 5. Experimental reflectivity curves for a DNA monolayer immersed in a TE−1 M NaCl buffer prepared with H_2O. Triangles: Adsorbed HS-ssDNA monolayer (Figure 1A). Circles: Same monolayer after hybridization without an intervening MCH treatment. The similarity of the two curves indicates little structural change.

of labile hydroxy protons for deuterons can shift the SLD of the terminal (−OD) groups closer to that of the D_2O buffer.[25] The expected width of the terminal −OD group region is about 0.2 nm, so that the total thickness of the MCH monolayer is estimated to be near 1.2 nm. This value agrees with independent ellipsometric measurements, which yielded 1.2 ± 0.1 nm assuming a refractive index of 1.45 for a pure MCH monolayer.

Following the MCH treatment, the HS-ssDNA layer in Figure 3 was hybridized to its complementary sequence, ssDNA-C. The hybridization step corresponds to going from model B to C in Figure 1. The volume fraction profile of the hybridized DNA is rather steplike (Figure 3 inset: dashed line), with an average volume fraction of about 7%. The total amount of DNA present is 0.8 mg/m^2,[18] corresponding to ∼100% hybridization efficiency. The hybridization is also reversible. When the sample is rinsed with 18 MΩ cm water, the hybridized strands separate, and the volume fraction profile assumes its prehybridization shape; however, re-exposure to the ssDNA-C hybridization solution results again in a flattened, steplike profile (data not shown). Additionally, as demonstrated previously with radiolabeling studies,[7] the hybridization of the mixed HS-ssDNA/MCH monolayers is sequence-specific, with essentially no binding of noncomplementary strands.

If the MCH treatment is omitted and hybridization of an adsorbed HS-ssDNA layer is attempted directly (from part A to part C of Figure 1), little change in reflectivity is observed (Figure 5). The difference in reflectivities is too small to allow reliable determination of variation in sample structure, but we estimate that 10% or less hybridization occurs. The lack of hybridization is consistent with surface-plasmon resonance studies of Piscevic et al.,[26] who reported 9% hybridization for nonspecifically adsorbed, 10-base-long HS-ssDNA oligonucleotides on gold. However, in ref 26, the surface densities of HS-ssDNA were an order of magnitude greater than those in the present study, and it is likely that electrosteric repulsions contributed to the lack of hybridization. In any case, it is clear from the present study that the end-tethered geometry (part B of Figure 1) can greatly improve hybridization yields compared to the nonspecifically bound HS-ssDNA (part A of Figure 1).

When hybridized, the DNA strands are no longer flexible. Rather, they become stiff and can be approximated as rigid cylinders. The distance along the chain backbone over which a strand of DNA will behave like a rigid rod is expressed by its persistence length,[19] which is ∼1.0 nm for single-stranded DNA[20] and around 80 nm for double-stranded DNA.[27] Because the contour length of the hybridized strands is 8.5 nm,[28] much less than the 80-nm persistence length, they can justifiably be regarded as rigid cylinders. The steplike profile of the hybridized DNA (Figure 3, dashed line) indicates that most of the cylinders possessed similar orientations; otherwise, the volume fraction profile should decrease more gradually from a maximum near the substrate to zero in the bulk. Interestingly, Figure 3 also shows that the hybridized DNA extends about 7.5 nm from the substrate (allowing for a 1.0-nm hexamethylene tether). Because this number is close to the full contour length, it implies that the hybridized strands adopted a preferential orientation toward the substrate normal despite the relatively low DNA volume fraction of 7%. The average angle between the surface normal and a double helix axis can be estimated as $\cos^{-1}(7.5/8.5) \approx 30°$. Possible causes of the preferentially perpendicular orientation are osmotic pressure due to mobile ions, steric/electrostatic interactions between the DNA helices, or both.

Osmotic pressure as a result of mobile ions arises because the ion concentrations (e.g., Na^+ and Cl^- ions) in the DNA layer and in the bulk are different. For example, Na^+ cations will be present in excess in the DNA layer in order to screen the negatively charged DNA backbones. The osmotic pressure originates from the tendency to minimize the gradients in ion concentrations between the surface and bulk regimes. To get an idea of the osmotic pressure force, we can model the DNA as a layer of immobile negative charges distributed uniformly over the surface region and apply a linearized Poisson−Boltzmann treatment from Borisov et al.[29] Integrating Borisov et al.'s eq A13 for the osmotic pressure force f_{OS} with respect to the layer thickness H yields the change in energy $\Delta F_{OS}/kT = -\int_i^f (f_{OS}/kT)\, dH$ due to mobile ions,

$$\Delta F_{OS}/kT = (Q/2)\ln[(n_f + 2n_B)/(n_i + 2n_B)] \qquad (1)$$

Equation 1 refers to the change in energy per single DNA cylinder. In the expression, kT is the thermal energy unit, n_B is the number density of ions in the bulk solution, and Q is the number of mobile counterions per DNA cylinder. Because of counterion condensation,[30] about 75% of the total number of 50 counterions per DNA helix should not be regarded as mobile so that $Q \approx 13$. Also, $n_i = Q/[\sigma H_i - V_C]$ and $n_f = Q/[\sigma H_f - V_C]$ are the number densities of mobile counterions attributable to DNA when the layer thickness is H_i or H_f, respectively. V_C is the DNA volume (assumed to be impenetrable to the ions), and σ is the surface area per cylinder. From the experimental data, the values of σ and n_B are 30 nm^2 and 6.0×10^{-1} nm^{-3} (1 M salt), respectively. Choosing the initial state to correspond to the perpendicular orientation (minimal F_{OS}) so that $H_i = 8.5$ nm and the final state to the experimentally observed $H_f = 7.5$ nm, we obtain $\Delta F_{OS}/kT \approx 0.05$. Although only approximate, this simple estimate indicates that at the 1 M salt conditions employed the osmotic pressure of the mobile ions is far from

(25) Labile protons on the DNA amine groups also undergo H−D exchange, shifting the bulk SLD of DNA from 3.4×10^{-4} to 4.2×10^{-4} nm^{-2} at full exchange. The exchange of the DNA protons does not affect the determination of the MCH layer thickness.

(26) Piscevic, D.; Lawall, R.; Veith, M.; Liley, M.; Okahata, Y.; Knoll, W. *Appl. Surf. Sci.* **1995**, *90*, 425−436.

(27) Bednar, J.; Furrer, P.; Katritch, V.; Stasiak, A. Z.; Dubochet, J.; Stasiak, A. *J. Mol. Biol.* **1995**, *254*, 579−594. To determine the persistence length, the authors of this study took particular care to use double-stranded DNA whose base sequence yielded intrinsically straight DNA rods.

(28) Sinden, R. S. *DNA Structure and Function*; Academic Press: New York, 1994.

(29) Borisov, O. V.; Zhulina, E. B.; Birshtein, T. M. *Macromolecules* **1994**, *27*, 4795−4803.

(30) (a) Manning, G. S. *Acc. Chem. Res.* **1979**, *12*, 443−449. (b) Manning, G. S. *Ber. Bunsen-Ges. Phys. Chem.* **1996**, *100*, 909−922.

sufficient to maintain the experimentally observed orientation. Even if a DNA cylinder is tilted so that it extends just 5 nm from the substrate, $\Delta F_{OS}/kT$ is still only 0.25. Therefore, we conclude that the orientation is a result of lateral interactions among neighboring helices.

A simple consideration can provide additional perspective. On average, the DNA cylinders are spaced about 6.0 nm apart center to center, and we estimate that because of electrostatic effects their effective diameter is ~3 nm. The effective diameter includes a ~0.5-nm-thick concentric sheath[30] of condensed counterions surrounding the 2.0-nm-thick helix. For a cylinder to come into contact with a perpendicularly oriented neighbor, it would have to tilt so that the lateral displacement of its free end, relative to a strictly perpendicular orientation, is on the order of 3 nm. The angle between the surface normal and the cylinder axis would therefore be $\sim\sin^{-1}(3/8.5) \approx 20°$, comparable with the experimental estimate of 30°. A more quantitative treatment could be obtained by extending statistical mechanical treatments of bulk liquid crystals[31] to charged, short rods tethered to a surface.

Conclusions

This report extends our earlier work with mixed alkanethiol/single-stranded DNA monolayers as model "DNA chips" for diagnostics applications[7] and clarifies the influence of surface chemistry and hybridization state on the monolayer structure. Monolayers of oligomeric DNA on gold surfaces have been characterized in situ using neutron reflectivity. DNA concentration profiles were obtained as a function of the distance from the substrate under high salt conditions (1 M NaCl). The results show that the formation of an alkanethiol (mercaptohexanol) monolayer in the presence of preadsorbed, single-stranded, thiol-terminated DNA can be used to control the DNA conformation and to yield terminally attached DNA strands. Furthermore, in the end-tethered geometry the DNA exhibits nearly 100% hybridization activity. Following hybridization, the double-stranded DNA helices were observed to preferentially orient toward the substrate normal. Additional issues, such as the effects of salt concentration and valency on the structure of DNA monolayers and the interaction of DNA monolayers with different analytes, are presently under investigation. Further studies will also facilitate additional comparison with other investigations of thiol end-tethered DNA monolayers on gold.[32−34] For instance, the location of an electrochemically active intercalator in a densely tethered double-stranded DNA monolayer[32] could be probed with neutron reflection techniques.

Acknowledgment. The authors thank Dr. Adam Steel (GeneLogic) and Dr. Nily Dan (University of Delaware) for helpful discussions. R.L. is a NIST/NRC Postdoctoral Research Associate. We also thank Dr. Stanley Abramowitz of the Advanced Technology Program at the National Institute of Standards and Technology for his support.

JA981897R

(31) For a summary of bulk liquid crystal theory, see: Odijk, T. *Macromolecules* **1986**, *19*, 2313−2329.

(32) Kelley, S. O.; Barton, J. K.; Jackson, N. M.; Hill, M. G. *Bioconjugate Chem.* **1997**, *8*, 31−37.

(33) Hashimoto, K.; Ito, K.; Ishimori, Y. *Anal. Chem.* **1994**, *66*, 3830−3833.

(34) Okahata, Y.; Matsunobu, Y.; Ijiro, K.; Mukae, M.; Murakami, A.; Makino, K. *J. Am. Chem. Soc.* **1992**, *114*, 8299−8300.